Applied Nanoscience (2024) 14:161–176
https://doi.org/10.1007/s13204-023-02970-8

ORIGINAL ARTICLE

From catalysis to combat: calix[4]pyrrole-wreathed palladium nanoparticles as ambidextrous tools against cancer and tuberculosis

Nandan C. Pomal[1] · Keyur D. Bhatt[1] · Anilkumar S. Patel[2] · Monil P. Dholariya[2] · Dinesh S. Kundariya[3] · Jaymin Parikh[1]

Received: 13 June 2023 / Accepted: 25 September 2023 / Published online: 10 October 2023

Abstract

Palladium nanoparticles (PdNPs) have gained significant importance due to its prodigious properties and applications. To harness the multifaceted applications of PdNPs, we report a facile synthesis of calix[4]pyrrole tetrabenzohydrazide capped-Palladium nanoparticles (CPTBH-PdNPs) through a one-pot synthetic pathway. Comprehensive characterization using UV–Visible spectroscopy, Transmission Electron Microscopy (TEM), Selected Area Electron Diffraction (SAED), Energy-Dispersive X-ray, X-ray Diffraction, Zeta Potential, and Dynamic Light Scattering techniques confirmed the successful formation of CPTBH-PdNPs. These nanoparticles were employed as catalysts in Suzuki–Miyaura coupling reactions under mild conditions, resulting in efficient bond formations. Furthermore, the CPTBH-PdNPs exhibited remarkable anti-cancer effects against the human breast cancer cell line MDA-MB-231, with an IC_{50} value of 38.86 µg/mL. Additionally, the nanoparticles demonstrated exceptional efficacy against *Mycobacterium tuberculosis*, with a minimum inhibitory concentration (MIC) value of 0.8 µg/mL. These findings highlight the multidimensional nature of calix[4]pyrrole capped PdNPs and suggest their potential application as future materials in various fields.

Keywords Anti-cancer · Calixarene · Calixpyrrole · Coupling reaction · Suzuki reaction · Tuberculosis

Introduction

Metal nanoparticles (MNPs), particularly transition metal nanoparticles (TMNPs) like palladium nanoparticles (PdNPs), have played a multifunctional role in various fields, including biology, environmental remediation, materials science, agriculture, medicine, and even space technology (Aksoy et al. 2023; Jamkhande et al. 2019; Javed et al. 2022; Pomal et al. 2021; Thangavelu et al. 2022). The unique properties of MNPs, such as facile functionalization, controlled size and shape, monodispersity, reactivity, large surface area to volume ratio, and stability, have led to novel discoveries in nanotechnology (Bhatt et al. 2021). Among TMNPs, PdNPs stand out for their exceptional catalytic activity and effectiveness in various C–C bond construction reactions, including the Suzuki, Hiyama, Negishi, Kumada, Heck, Sonogashira, Stille, and more (Budarin et al. 2010). These reactions have found wide applications in the synthesis of active pharmaceutical ingredients, agrochemicals, and fine chemicals, thanks to the mild reaction conditions, environmentally friendly boronic acid derivatives, and the ease of processing and eliminating boron-containing residues compared to other organometallic reagents (Ayogu and Onoabedje 2021; Kotha et al. 2002; Liu et al. 2021; Pérez-Lorenzo 2012).

Suzuki–Miyaura reactions use haloarenes and boronic acid derivatives of arenes, along with base to generate biaryls in high yields using various palladium substances, including ligated complexes, salts, nanoparticles, etc., amongst which some substances are subject to demonstrating sensitivity towards air and moisture, which results in deactivation of the surface of catalysts and retardation of reactions (Bedford and Cazin 2001). Thus, contrary to Pd(II)/Pd(0) ligand-based complexes, PdNPs catalyzed reactions are substantially cost-effective, promote an easy

✉ Keyur D. Bhatt
drkdbhatt@outlook.com; kdb01@guni.ac.in

[1] Department of Chemistry, Faculty of Science, Ganpat University, Kherva, Mehsana, Gujarat, India

[2] Department of Chemistry, Atmiya University, Rajkot, Gujarat, India

[3] Department of Chemistry, Tolani College of Arts and Science, KSKV Kutch University, Bhuj, Gujarat, India

work-up process, allow smoother isolation of final products, facilitate the facile recovery of nano-catalysts, and give a high yield in less time (Pérez-Lorenzo 2012). These nanoparticles have demonstrated positive results in various discoveries, including their potential as anti-cancer agents and their effectiveness against tuberculosis (TB).

There were near 2.3 million new instances of breast cancer in 2020, with approximately 685,000 deaths due to this. It is anticipated that by 2040, population growth and aging will generate over 3 million new cases and 1 million fatalities annually (Melina Arnold et al. 2022). To combat this, new anti-cancer drugs are being investigated to avoid adverse effects and drug resistance associated with existing therapies. MNPs have shown promising results to tackle the cancerous cells with excellent results (Bandyopadhyay 2020; Banerjee et al. 2019), and amongst which palladium nanoparticles have demonstrated positive results in various discoveries (Gil et al. 2018; Guleria et al. 2023; Othman 2020). Tuberculosis is the second most contagious illness globally, with millions of reported cases and significant mortality rates, and according to WHO, in 2021, 1.6 million individuals lost their lives by TB globally and nearly 10.6 million cases reported worldwide ((WHO) 2023). The current therapies for TB, including prolonged medical care and complex drugs, often come with severe side effects and high costs (Alzahabi et al. 2020; Merk et al. 2019) which have induced the need to discover alternatives against the current therapies in which metal nanoparticles may provide promising results (Richa Singh et al. 2016).

In view of this, the new tetrabenzohydrazide functionalized calix[4]pyrrole CPTBH is reported that has been employed to synthesize monodispersed, highly stable, and catalytically active palladium nanoparticles (CPTBH-PdNPs) by a one-pot synthetic procedure. The greater stability, efficiency, strength and controlled encapsulation of PdNPs are attributable to non-covalent hydrogen bonding by four pyrrole groups, the web-like cavity of calix[4] pyrrole molecules and electron-withdrawing nature of hydrazide groups (Bhatt et al. 2016), which enables the multiple coordination sites for palladium nanoparticles (Kongor et al. 2016). In contrast to certain other ligands, the CPTBH has characteristics nature of befitting, eloquent, and inexpensiveness, that also possess the twin advantage of reductant and stabilizer to PdNPs. It is possible to assert that the integration of the physicochemical attributes of nano-palladium and powerful encapsulating feature of CPTBH has propitious outcomes as a catalyst for extremely advantageous C–C coupling reaction, and exhibited promising cytotoxicity for MDA-MB-231 cells and possess anti-tuberculosis efficacy for the first time to the best of our knowledge.

Materials and methods

Chemical reagents

The 4-acetyl benzoic acid, pyrrole, hydrochloric acid, hydrazine hydrate, and palladium chloride exploited in the research were all analytical rank, purchased from Sigma-Aldrich. Other chemicals and solvents were bought from a nearby supplier and used directly. Merck provided fluorescent active (F-254) TLC plates. Remi (2 MLH) magnetic stirrer have been used in a synthetic operation, and all glass-wares were calibrated before any experiments were conducted. MDA-MB-231 was the cell line utilized in the cytotoxicity experiment. Hypoglycemic DMEM (Dulbecco's Modified Eagle Media) cell culture (Gibco, Invitrogen Cat. No. 11965-092). Antibiotic–Antimycotic 100 × solution (Cat. No. 15240062, Thermofisher Scientific), FBS (Fetal Bovine Serum) (Cat. No. 10270106, Gibco, Invitrogen). Doxorubicin is a positive control. As a negative control, untreated media-filled cells were employed. *Mycobacteria tuberculosis* (Vaccine strain, H37 RV strain): ATCC No-27294 used as standard strain for anti-TB assay. Isoniazid, Ethambutol, Pyrazinamide, Rifampicin, and Streptomycin used for comparison of anti-TB data of CPTBH-PdNPs.

Instruments

Uncorrected melting points were determined using a 97 VEEGO apparatus (VEEGO, Mumbai, India). An infrared spectrum of all compounds, acquired by virtue of Bruker FT-IR, ALPHA-II. UV–Visible (model SHIMADZU-1900) portrayed the UV graph. ChemDraw Professional software was exerted to generate structures and nomenclature of compounds. The Transmission Electron Microscope, Energy-Dispersive X-ray as well as Surface Area Electron Diffraction (model name JEOL, JEM-2100) and Scanning Electron Microscope (JEOL, JSM 7100F) have functioned to create images to examine the morphology and size of CPTBH-PdNPs. For Powder X-ray analysis Philips X'pert MPD System (3 kW) utilized. With a Brucker ASCENDTM-400 instrument, NMR spectra were recorded. The SHIMADZU Nexera 2020 and HORIBA SZ-100 instruments were used to measure the ESI–MS spectrum and Zeta potential of the CPTBH-PdNPs, respectively.

Scheme 1. Synthesis of CPTBA

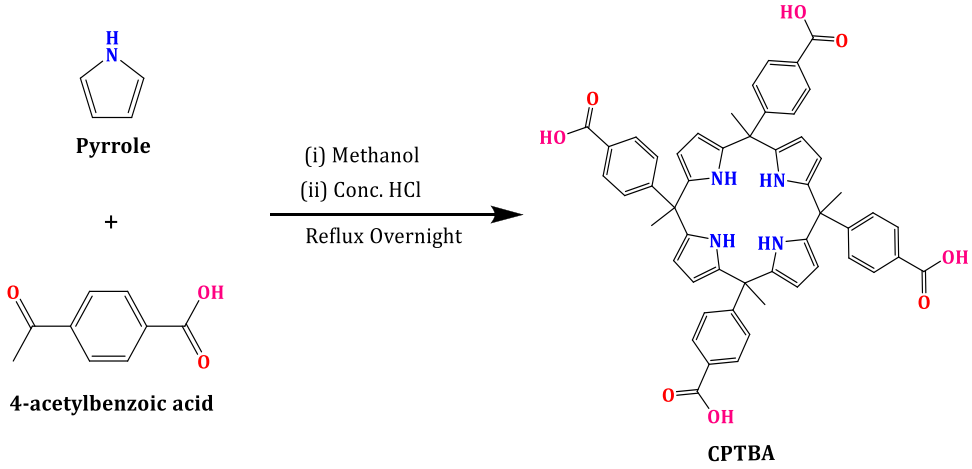

Synthesis

Synthesis of tetrabenzoic acid derivative of calix[4]pyrrole (CPTBA)

A reported procedure (Desai 2022) was altered slightly to produce the tetrabenzoic acid derivative of calix[4]pyrrole (CPTBA) via concentrated hydrochloric acid catalyzed condensation of pyrrole with 4-acetyl benzoic acid. Under standard laboratory setup, a 4-acetyl benzoic acid (0.41 g, 25 mmol) was made soluble in 50 mL of methyl alcohol in a flask with a round bottom. Subsequently, a highly purified pyrrole (0.17 mL, 25 mmol) was introduced dropwise to the 4-acetyl benzoic acid solution. For 15 min, the mixture was swirled on a magnetic stirrer while heating. This reaction mixture received a drop-by-drop transfer of 1.0 mL of concentrated hydrochloric acid, which was completed in 15–20 min, followed by an overnight agitation at reflux. After the reaction was finished, 200 mL of frigid water was poured in to the mixture, the dark brown precipitates appeared immediately when a few drops of triethylamine were added. The precipitates were dissolved in diethyl ether and this solution was passed through a bed of anhydrous sodium sulfate to remove any moisture present in the product. Reduced pressure was maintained on a solution to obtain a solid crude product. A column chromatography was adopted to procure high purity of compound by silica (60–120 mesh) as the stationary phase and chloroform:methanol (8:2) was employed as an eluent. The fractions were separated quickly, and from that major product was isolated using n-hexane (3 × 10 mL) which yielded dark brown solid powder CPTBA (Scheme 1).

Dark brown solid (63% yield). M.P.: 278–280 °C. Chemical Formula: $C_{52}H_{44}N_4O_8$. Elemental Analysis: C (73.23%); H (5.20%); N (6.57%); O (15.01%). FT-IR: (KBr disk): 3400, 1714 cm^{-1}. ^{1}H-NMR (400 Mega Hertz, d6-DMSO): (δ in ppm) = 1.99 (s, 12H, CH_3), 5.93 (d, 8H, Pyrrolic CH, ArH), 7.08 (d, 8H, Benzene CH, ArH), 7.92 (d, 8H, Benzene CH, ArH) 9.94 (s, 4H, Pyrrolic NH), 11.89 (s, 4H, OH). ^{13}C-NMR (125 MHz, MeOH-d_4) δ = 169.76, 150.05, 142.65, 131.41, 131.34, 129.26, 109.96, 52.30, 29.38. ESI–MS (*m/z*): 852.6 g/mol.

Synthesis of tetrabenzohydrazide derivative calix[4]pyrrole (CPTBH)

In a 50 mL of pure ethanol, a CPTBA (0.5 g, 0.55 mmol) was solubilized to which gradual addition of hydrazine hydrate (0.82 mL, 17 mmol) was finished in order to produce the novel tetrabenzohydrazide derivative CPTBH. For 72 h, the reaction mixture was refluxed while being alternately monitored using a thin-layer chromatography plate. A reaction mixture was combined with a large volume of cold water once the reaction was complete, and gradually yellowish-brown precipitations appeared in powder form. In order to remove moisture from the chemical, this compound was solubilized in methanol, and then passed over a bed of anhydrous sodium sulfate. The solution was then extracted using less pressure. The crude product was recrystallized in hot methanol, producing a yellowish-brown powder called meso-tetra(methyl) meso-tetra(benzohydrazide), a tetrabenzohydrazide derivative calix[4]pyrrole CPTBH (Scheme 2).

Yellowish-brown solid (53% yield). M.P.: 202–204 °C. Chemical Formula: $C_{52}H_{52}N_{12}O_4$. Elemental Analysis: C (68.70%); H (5.77%); N (18.49%); O (7.04%). FT-IR (KBr disk): 3317, 1671, 1274, 1179 cm^{-1}. ^{1}H-NMR (400 Mega Hertz, d_6-DMSO): (δ in ppm) = 1.99 (s, 12H, CH_3), 4.29 (s, 8H, NH_2), 5.93 (d, 8H, Pyrrolic CH, ArH), 7.15 (d, 8H, Benzene CH, ArH), 7.82 (d, 8H, Benzene CH, ArH) 9.90 (s, 4H, Pyrrolic NH), 10.40 (s, 4H, NH). ^{13}C-NMR (125 MHz, MeOH-d_4) δ = 167.77, 149.04, 141.56, 135.22–124.24 (m), 110.69, 52.10, 26.29. ESI–MS (*m/z*): 908.4 g/mol (Fig. 1).

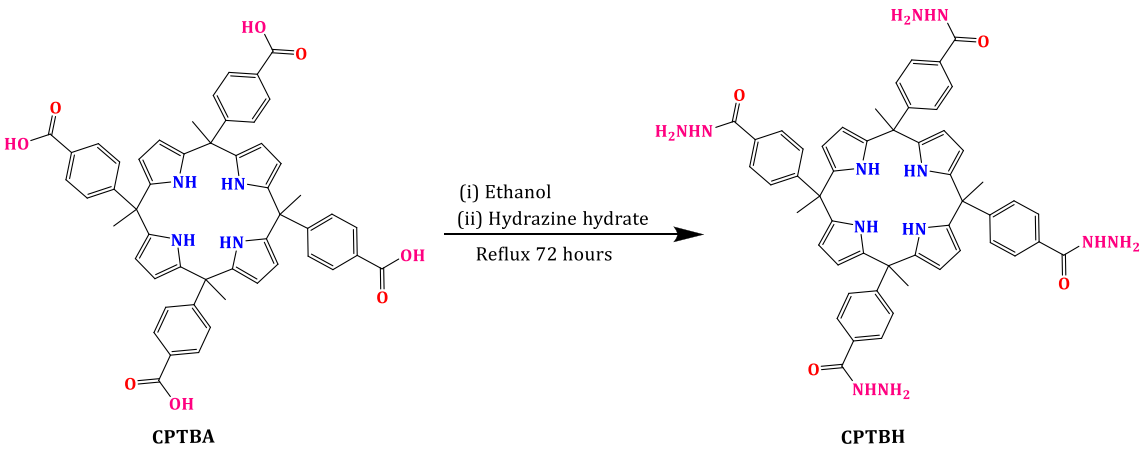

Scheme 2. Synthesis of CPTBH

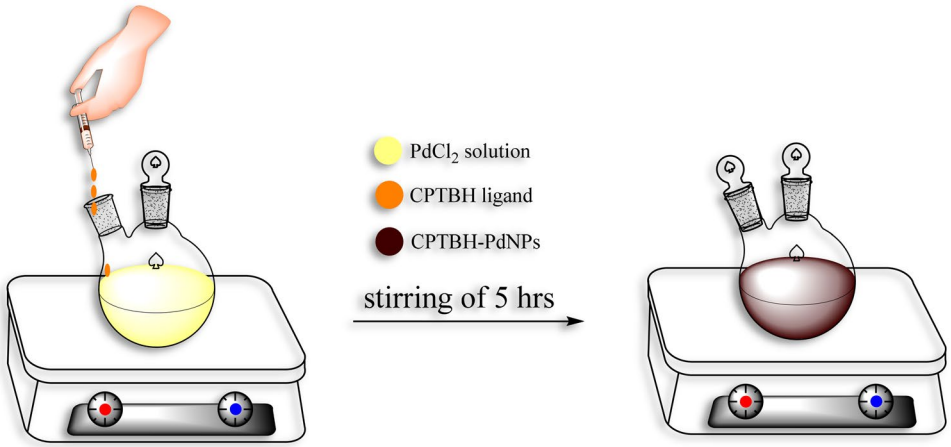

Fig. 1 Schematic representation of preparation of CPTBH-PdNPs

Synthesis of CPTBH-capped palladium nanoparticles (CPTBH-PdNPs)

With palladium chloride as a salt precursor, a one-pot synthesis strategy was chosen to fabricate extremely stable CPTBH-capped PdNPs. Before succeeding to achieve the final CPTBH-PdNPs solution, different volumes and concentrations of ligand and salt precursor were examined in which, the volume of 1.0 mM $PdCl_2$ (100 mL) vigorously stirred for 20 min at temperature 60 °C. Following this, 1.0 mM CPTBH (20 mL) was gradually added to a heated solution of $PdCl_2$. In the next 30 min, the yellow colour of the solution was slowly turned to brownish-black, authenticated the characteristics colour of palladium nano-colloids, this mixture was swirled continuously for 5 h to obtain monodispersed, spherical and uniform-sized CPTBH-PdNPs and this solution was subsequently maintained at a temperature of 4 °C for further investigation. The CPTBH-PdNPs were then examined by UV–Visible spectrophotometry for the confirmation of the absence of characteristics peak of $PdCl_2$.

Cytotoxicity action of CPTBH-PdNPs upon MDA-MB-231 cell line by MTT assay

Principle

This colorimetric test evaluates the degree to which mitochondrial succinate dehydrogenase reduces the yellow 3-(4,5-dimethythiazol-2-yl)-2,5-diphenyl tetrazolium bromide (MTT). The MTT penetrates the cells and travels to the mitochondria, where it is converted to a formazan product which is dark purple in colour and insoluble. The released, solubilized formazan reagent is evaluated spectrophotometrically after the cells have been solubilized with an organic solvent (such as DMSO or isopropanol). The amount of activity is a measure of the viability of the cells since reduction of MTT only occur in cells that are metabolically active.

Procedure for assessment of cytotoxicity of CPTBH-PdNPs on MDA-MB-231 cell line

Under the special conditions of 37 °C temperature (maintained), 95% humidity and 5% CO_2, MDA-MB-231 cells were sown in 96-well flat bottom microplate for entire night. CPTBH-PdNPs had been administered in various concentrations (100, 50, 25, 12.5, 6.25, and 3.125%), and then another 48 h were spent incubating the cells. Phosphate Buffered Saline (PBS) was used to rinse the wells two times. After that, in each well, an MTT staining (volume of 20 µL) was injected, and then plate was allowed to incubate at 37 °C. In order to dissolve the formazan crystals, 100 µL of DMSO was introduced to each well after 4 h had passed. A microplate reader was used to measure the absorbance at a wavelength of 570 nm, the calculation for the percentage of MDA-MB-231 cells that survived was done using following formula;

$$\text{Surviving cells}(\%) = \frac{\text{Mean OD of test compound}}{\text{Mean OD of Negative control}} \times 100.$$

MABA for anti-tuberculosis (anti-TB) activity of CPTBH-PdNPs

The approach showcases good concordance with proportional and BACTEC radiometric methods, is non-toxic, and involves highly stable thermal reagents (Lourenco et al. 2007). In order to reduce the amount of medium that evaporates out in the test wells during incubation, 200 µL of deionized water that was sterile was administered across every of the sterile 96-well plates outside the perimeter wells. The Middlebrook 7H9 broth was added to the 96-well plate at a volume of 100 µL, and the compounds were serially diluted right there on the plate. The final dosages of drugs assessed were in the range of 100–0.2 µg/mL. Parafilm had been applied to laminate and seal the plates, which were subsequently left to incubate at 37 °C over 5 consecutive days. Following this, the plate received 25 µL of freshly prepared 1:1 Alamar Blue reagent and 10% tween 80, which then underwent incubation for 24 h. A well that was blue was interpreted to have no bacterial growth, in contrast to a well that was pink was rated to have a growth. The minimum inhibitory concentration (MIC) was defined as lowest drug concentration which prevented the color change from blue to pink.

Results and discussion

Characterization

Metal nanoparticle characterization is a key step in understanding their properties and behavior in applications where they will be exploited. The spectroscopic techniques such as UV–Visible, TEM (Transmission Electron Microscopy), EDX (Energy-Dispersive X-ray), SAED (Selected Area Electron Diffraction), Zeta Potential and DLS (Dynamic Light Scattering) are primary methods used for the characterization of metal nanoparticles.

UV–Visible method has been used in broadways to examine and ratify constitution of the metal nanoparticles. An absorbance peak of $PdCl_2$ surrounding 400 nm in the UV–Visible spectrum (Fig. 2) has confirmed the existence of Pd(II) ions; on this side, In general, in a visible region, a colloidal nano-palladium lacks a noticeable Surface Plasmon Resonance (SPR) band (Creighton and Eadon 1991; Modi et al. 2019). Therefore, an extinction of signal of $PdCl_2$ from about 400 nm (Fig. 2) verified the complete conversion of Pd(II) to Pd (0) by tetrabenzohydrazide calix[4]pyrrole ligand (Nemamcha et al. 2006). The CPTBH-PdNPs are found to be stable for more than 180 days in the monodispersed state without any aggregation and stability of CPTBH-PdNPs is shown in Fig. 3a, b.

A transmission electron microscopy (TEM) method produces high-resolution images of nanoparticles. TEM pictures were immensely beneficial in examining the dispersion, morphology, and size of CPTBH-PdNPs. In a typical method, a carbon-coated copper grid was placed on filter paper and a drop of the CPTBH-PdNPs solution was placed on the grid, which was subsequently introduced into the device after having dried out at ambient temperature. According to the findings, the sample of CPTBH-PdNPs was found to be monodispersed, having mean size 14 ± 2 nm and roughly spherical in shape (Fig. 4a, b). SAED technique delivered the four concentric rings with intense bright spots produced which endorsed crystalline natured CPTBH-PdNPs (Fig. 4c) providing a visual representation of this.

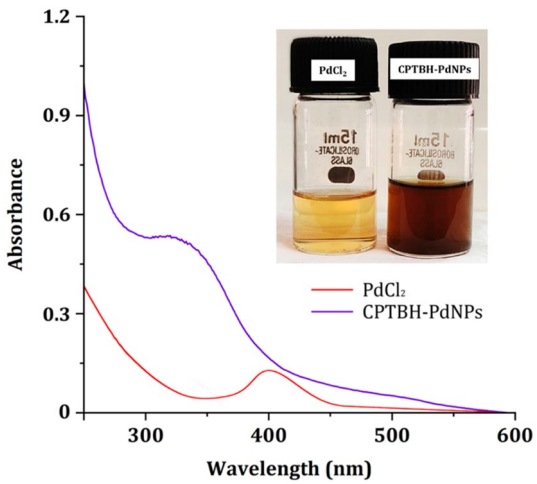

Fig. 2 UV–Visible spectrum of CPTBH-PdNPs

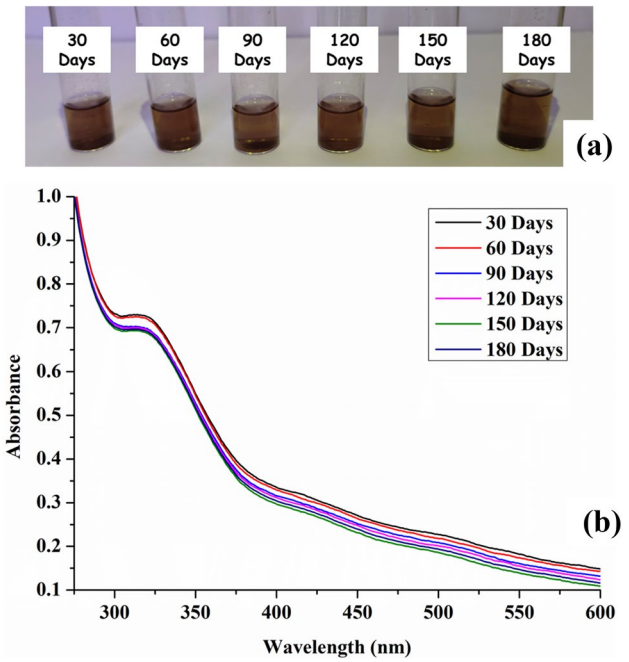

Fig. 3 **a** Monodispersed CPTBH-PdNPs and **b** UV–Visible spectra on different time gap

A Scanning Electron Microscopy (SEM) imaging enables reliable evaluation of size, shape, and distribution of CPTBH-PdNPs for the organic synthesis in Suzuki–Miyaura C–C coupling reaction. The SEM analysis conforms the surface of coarsely granular, which may provide the catalysis on its surface with the distinct resolution on scale bar of 100 nm with 10 k, 30 k and 90 k zoom (Fig. 5a–c).

Powder X-ray Diffraction (Powder XRD) is a valuable technique for characterizing functionalized PdNPs, revealing crystallographic characteristics and structural alterations caused by functionalization. In XRD peaks expressed in Fig. 6 at $2\theta = 40.33°$, 46.85°, 68.33°, 82.15°, and 86.48° in accordance to d-spacing values of 2.34, 2.03, 1.37, 1.17 and 1.13 Å, respectively, as well as these values are in agreement with the (111), (200), (220), (311) and (222) crystallographic lattice planes of FCC.

Another approach used to determine the elemental composition of the nanoparticles is EDX. Palladium in an elemental form shown to be present in an EDX technique (Fig. 7a), which was analyzed on the TEM grid. The zeta potential of nanoparticles serves to quantify how uniformly MNPs disperse in a solution, and it ranges from + 30 mV to − 30 mV (Barhoum et al. 2018). In the present work, DLS (Dynamic Light Scattering) result reveals the hydrodynamic diameter of CPTBH-PdNPs to be 44.4 nm (Fig. 7b) which is because of surface functionalization of CPTBH ligand over the core PdNPs and zeta potential was found to be − 27.6 mV (Fig. 7c), which implies a greater level of stability and a negative value facilitated by the negative-charged ligand CPTBH capping on PdNPs.

Along with that, Table 1 shows the comparison of bared and pure nanoparticles with spherical morphology and size ranges from that some of them exhibiting catalysis applications.

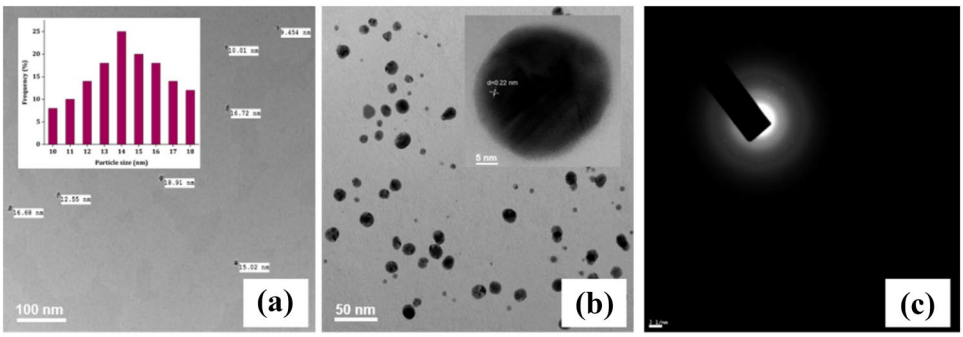

Fig. 4 **a** TEM image of CPTBH-PdNPs scale bar 100 nm (inset: particles size distribution), **b** HRTEM image of CPTBH-PdNPs scale bar 50 nm (inset: image of 5 nm scale bar), and **c** SAED image of CPTBH-PdNPs

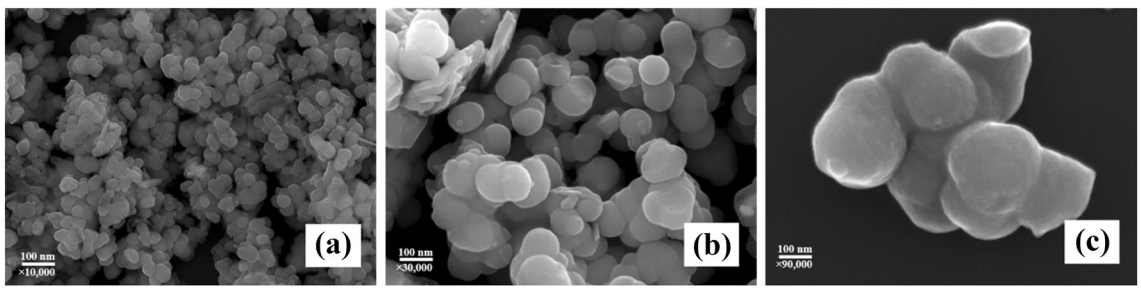

Fig. 5 SEM images of CPTBH-PdNPs on scale bar of 100 nm with different resolutions

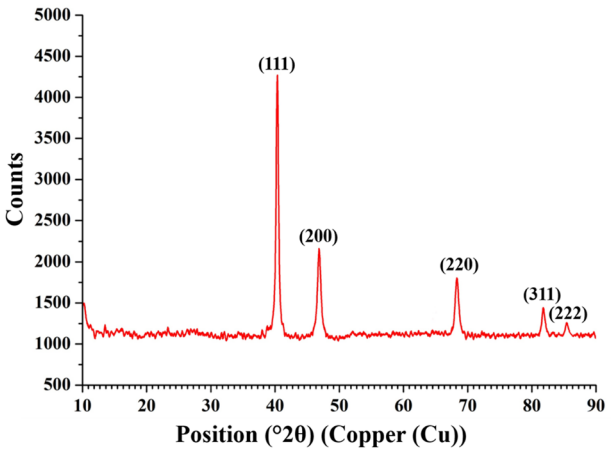

Fig. 6 Powder X-ray pattern of CPTBH-PdNPs

Capping mechanism of tetrabenzohydrazide calix[4]pyrrole on palladium nanoparticles (CPTBH-PdNPs)

The exact chemistry of capping behaviour of calix[4]pyrrole on metal nanoparticles is perplexing, and concurrently the functionalization of PdNPs by the CPTBH process can depend on a range of factors, including ligand concentration, reaction parameters, nanoparticle morphology and size, and kind of ligand and its character. Hence, various prospects that can help to eradicate the ambiguity surrounding this discussion. In the present study, the interactions between the palladium nanoparticles and the CPTBH ligand, and the role of the ligand in stabilizing the nanoparticles can be explained by considering the above factors with past studies.

According to studies, the reducing and capping behaviour on the surface of PdNPs by calix[4]pyrrole tetrabenzohydrazide involves the adsorption of the ligand onto the

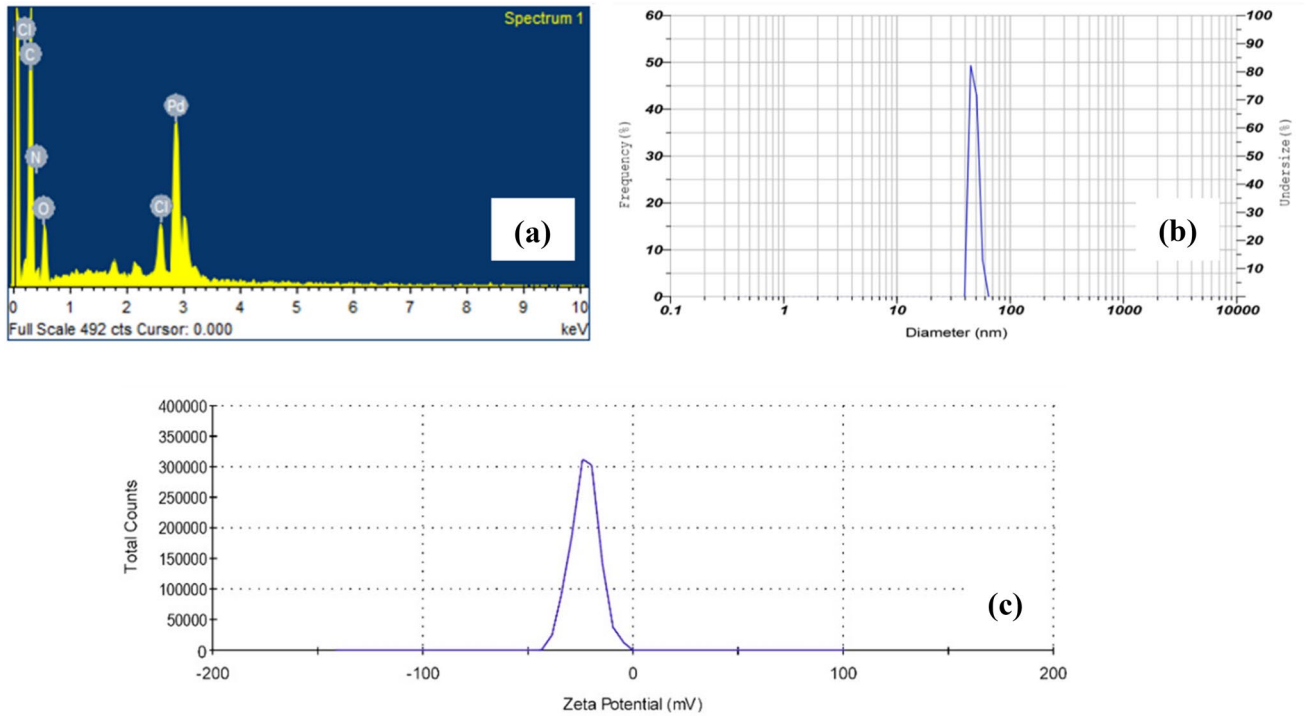

Fig. 7 **a** Energy-dispersive X-ray image and **b** dynamic light scattering image, and (c) Zeta potential image of CPTBH-PdNPs

Table 1 Comparison of CPTBH-PdNPs with bare PdNPs

S. no.	Palladium nanoparticles type	Applications	Shape	Size (in nm)	References
1	Bare PdNPs	Catalyst in olefin hydrogenation reactions	Spherical	12.7 ± 5.7	(Hwang et al. 2000)
2	Bare PdNPs	Catalyst in reduction of 4-nitrophenol	Spherical	Not mentioned	(Liu et al. 2018)
3	Pure PdNPs	Not applicable	Spheroidal	5.0–15.0	(Cristoforetti et al. 2011)
4	Bare PdNPs	Catalyst in dye reduction of methylene blue dye	Spherical	7.89–13.10	(Wang et al. 2021)

surface of the nanoparticles, as well as hydrogen bonding, van der Waals, and electrostatic interactions may all contribute (Chen et al. 2013; Ha et al. 2009). Modi et al. and Kongor et al. carried out detailed computational investigations to understand the capping mechanism of hydrazide functionalized macrocyclic ligand, in which through computational models, it was elucidated that ligands could interact with the metal surface through pi-stacking interactions, while the hydrazide groups can form hydrogen bonds with the metal surface, once adsorbed onto the surface of the nanoparticles, nitrogen atoms on hydrazide groups of CPTBH form the Pd–N bonds (Kongor et al. 2018b; Modi et al. 2019). In the present case, the formation of these bonds can be facilitated by the lone pair of electrons on the nitrogen atom which may then transferred from ligand to metal which is responsible for the reduction of palladium ions to atomic palladium and ultimately stabilizes the PdNPs (Bhatt et al. 2014; Kongor et al. 2019; Modi et al. 2019; Newman and Blanchard 2006), as a result, a protective layer of CPTBH formed on the metal surface can prevent the aggregation and oxidation of the PdNPs while also improving their catalytic capabilities.

Catalytic action of CPTBH-PdNPs in a Suzuki–Miyaura coupling

During the past few years, PdNPs as rate accelerator in Suzuki–Miyaura reaction endeavors a great achievement owing to their improved stability, enhanced catalytic activity, selective catalysis, versatility, and reusability (Hong et al. 2020; Narkhede et al. 2019; Pérez-Lorenzo 2012). To acquire exquisite findings, several factors have to be controlled critically, namely reaction conditions, choice of base, variations in temperature, solvent selection, and concentration of nano-catalyst (Marziale et al. 2010; Miyaura 2002).

Within this framework, the CPTBH-PdNPs were investigated for the cross-coupling reaction among bromobenzene and phenylboronic acid (both in 1.0 mmol) using the best optimal reaction parameters, i.e. K_2CO_3 (2.0 mmol) as a base, 2.0 mL of dimethylformamide (DMF) as solvent, 0.008 mmol concentration of CPTBH-PdNPs, 80 °C temperature, and time of 30 min that yielded 97% of the final product (Table 2). In addition, to confirm the parallels in findings under optimal circumstances, the breadth of the work was also examined for various electron-deficient and neutral aryl halides with the same phenylboronic acid. The reactions were carried out satisfactorily, with cross-coupled products as the major ones (Table 3). ^{1}H-NMR and Mass spectrometry methods were employed to characterize the compounds synthesized are mentioned in Supporting data file.

The catalytic activity of CPTBH-PdNPs

The catalytic activity of PdNPs depends on a range of factors, comprising particle size, shape, structure, surface area (active sites), surface chemistry, and so forth (Chatterjee and Bhattacharya 2018; Chen and Ostrom 2015; Pérez et al. 2012). On account of these, the catalytic activity of CPTBH-PdNPs was supposed to review with the Suzuki–Miyaura coupling reaction.

The Suzuki coupling reaction of bromobenzene with phenylboronic acid was investigated as model reaction for the optimization of experimental conditions including solvents, catalyst and reaction temperature (Table 2).

Initially, the necessity of palladium as a catalyst in the Suzuki coupling was illustrated at the beginning via performing the reaction without palladium catalyst with DMF at 80 °C and K_2CO_3 as a base in 2 h without forming the product (Table 2, entry 1), afterward in support of need of catalyst in the reaction, the reactions were carried out in presence of $PdCl_2$ with same reagents used above which gave 44% output (Table 1, entry 2). Next, the model reaction was repeated in the presence of CPTBH-PdNPs (0.008 mmol) and various bases such as K_2CO_3, Na_2CO_3, Et_3N, KOH and CH_3COONa in combination with different solvents such as acetone, THF, DCM, toluene, dioxane, DMF and ethanol under appropriate temperature condition (Table 2, entry 3–13). Off these, K_2CO_3 as base in DMF under the presence of CPTBH-PdNPs as a catalyst served as better condition to give excellent yield (Table 2, entry 8). The optimum concentration of catalyst required for coupling reaction also assessed by changing concentration of CPTBH-PdNPs catalyst (0.007–0.010 mmol) showed lower yield in lower concentration of catalyst (Table 2, entry 14) and showed minor deviations in product yield with higher concentration (Table 2, entry 8, 15 and 16). In temperature variations poor to promising results were obtained from lower to intermediate to high temperature (Table 2, entry 8, 17–22) as well as in time alteration the lower yield of product formed due to generation of several impurities (Table 2, entry 23, 24). Thus, it can be reported that the reaction between bromobenzene and phenylboronic acid yielded 97% of biphenyl in the presence of 0.008 mmol CPTBH-PdNPs catalyst in DMF solvent and K_2CO_3 as a base at 80 °C in 30 min.

After optimization of reaction condition, in the next step, Suzuki coupling reaction of variety of aryl bromides with phenyl boronic acid was performed to explore the scope of the protocol. The results are represented in Table 2. As expected, coupling reaction of aryl bromides contains electron donating group as well as electron-withdrawing

Table 2 Suzuki–Miyaura reaction of bromobenzene with phenylboronic acid in various optimized conditions

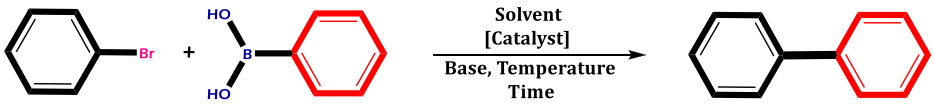

bromobenzene **phenylboronic acid** **1,1'-biphenyl**

Entry	Solvent	Catalyst CPTBH-PdNPs (mmol)	Base	Temperature (°C)	Time (min.)	Yield (%)
1	DMF	Catalyst not used	K_2CO_3	80	120	No product formation
2	DMF	$PdCl_2$ (0.008)	K_2CO_3	80	100	44
3	*Acetone*	*0.008*	*K_2CO_3*	*60*	*50*	*88*
4	*THF*	*0.008*	*K_2CO_3*	*60*	*50*	*40*
5	*DCM*	*0.008*	*K_2CO_3*	*40*	*90*	*38*
6	Toluene	0.008	K_2CO_3	80	60	50
7	1,4-dioxane	0.008	K_2CO_3	80	40	80
8	DMF	0.008	K_2CO_3	80	30	97
9	Ethanol	0.008	K_2CO_3	80	35	85
10	DMF	0.008	Na_2CO_3	80	45	87
11	DMF	0.008	Et_3N	80	40	70
12	DMF	0.008	KOH	80	60	65
13	DMF	0.008	CH_3COONa	80	95	50
14	*DMF*	*0.007*	*K_2CO_3*	*80*	*30*	*70*
15	*DMF*	*0.009*	*K_2CO_3*	*80*	*30*	*94*
16	*DMF*	*0.010*	*K_2CO_3*	*80*	*30*	*95*
17	DMF	0.008	K_2CO_3	60	30	50
18	DMF	0.008	K_2CO_3	70	30	62
19	DMF	0.008	K_2CO_3	90	30	88
20	DMF	0.008	K_2CO_3	100	30	95
21	DMF	0.008	K_2CO_3	110	30	94
22	DMF	0.008	K_2CO_3	120	30	94
23	DMF	0.008	K_2CO_3	80	100	70
24	DMF	0.008	K_2CO_3	80	250	65

Reaction conditions Bromobenzene (1.0 mmol), Phenylboronic acid (1.0 mmol), DMF (2.0 mL), K_2CO_3 (2.0 mmol) CPTBH-PdNPs (in mmol), Temperature (in °C)

group with phenylboronic acid gives more than 90% yields (Table 3, entry 2–7). Table 4 below shows the relative data of different calixarene capped palladium nanoparticles as catalysts used in Suzuki coupling reactions for comparing a present studies outcomes with past studies.

Recyclability

The significance of the recyclability of palladium nanoparticles in cross-coupling reactions can be attributed to its myriad advantages; such as being more environment-friendly and sustainable by reducing the sheer amount of debris produced, it minimizes the cost of the reaction altogether in terms of an industrial perspective. Moreover, the recyclability of palladium nanoparticles enables the use of milder reaction conditions, which can lead to higher yields and fewer by-products.

Palladium nanoparticles in general possess excellent recyclability and recoverability in C–C coupling reactions irrespective of several cycles of catalysis (Shakil Hussain et al. 2019). Hence, the recyclability of CPTBH-PdNPs was studied in this regard. On centrifugation, CPTBH-PdNPs were simply separated out from reaction blend, and rinsed with deionized water (4 × 5 mL) as well as diethylether (4 × 5 mL) to get off any organic compound, which was then air dried for 24 h after being filtered off the product using filter paper.

Following that, the recovered catalyst was immediately employed in a second coupling experiment. Similarly, a CPTBH-PdNPs was re-employed in the coupling reaction for

Table 3 Bromoarenes with phenylboronic acid in Suzuki–Miyaura coupling catalyzed by CPTBH-PdNPs

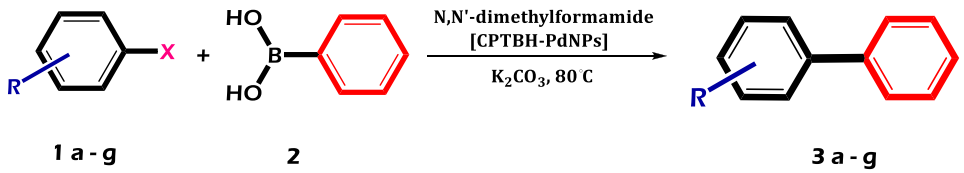

Entry	Aryl bromides	Time (min)	Product[b]	Yield[c] (%)	Melting point (°C)	
					Found	Reported [ref]
1	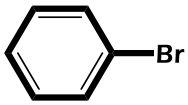	30	**3a**	97	70–72	69–71 (Mukhopadhyay et al. 2002)
2	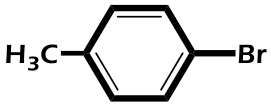	30	**3b**	96	46–48	47–48 (Percec et al. 1995)
3		35	**3c**	90	86–87	85–86 (Chen et al. 2014)
4	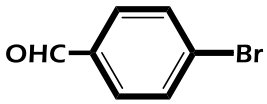	35	**3d**	93	59–61	60–61 (HironaoSajiki et al. 2005)
5	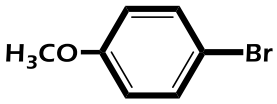	30	**3e**	91	86–88	87–88 (HironaoSajiki et al. 2005)
6	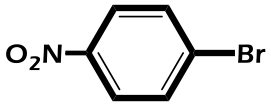	40	**3f**	90	112–114	113–114 (HironaoSajiki et al. 2005)
7	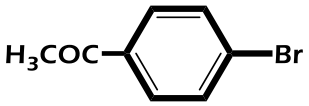	35	**3g**	92	118–120	119–121 (HironaoSajiki et al. 2005)

[a]Reaction condition: Bromoarenes and Phenylboronic acid (each with 1.0 mmol), CPTBH-PdNPs (0.008 mmol), K_2CO_3 (2.0 mmol) in DMF (2.0 mL) at 80 °C. [b]Characterization of each compound was executed deploying Melting Point, Mass, IR, ^{1}H-NMR, etc. and compared with reported data. [c]Isolated yields

Table 4 Comparison of different calixarene enabled PdNPs catalyzed C–C coupling reactions

S. no.	Catalyst	Particle size	Reaction time	Product yield (%)	References
1	Thiacalixphenyl[4]arene tetraacetohydrazide-PdNPs	4 ± 2 nm	10 min	95	(Modi et al. 2019)
2	5,17-di(hydrazinecarbonyl) tetranitrooxacalix[4]arene-PdNPs	5 ± 2 nm	20 min	92	(Mehta et al. 2016)
3	Tetramethoxy resorcinarene tetrahydrazide-PdNPs	5 ± 2 nm	10 min	94	(Panchal et al. 2016)
4	Oxacalix[4]arenedihydrazide-PdNPs	3–4 nm	60 min	98	(Panchal et al. 2018)
5	Calix[4]pyrrolesoctahydrazide-PdNPs	16 ± 2 nm	15 min	94	(Bhatt et al. 2021)
6	Tetraallyl calixarene(MCM-allylcalix)-PdNPs	12 ± 2 nm	6 h	96	(Narkhede et al. 2019)
7	Calix[4]pyrrole tetrabenzohydrazide-PdNPs	14 ± 2 nm	30 min	97	Current study

five consecutive cycles with no appreciable loss in catalytic potency. Howbeit, after the sixth cycle there observed an aggregation and decrement in the catalytic power (Fig. 8a). Ultimately, it can be said that CPTBH-PdNPs have performed excellently withstanding the five consecutive cycles in the Suzuki–Miyaura C–C coupling transformations with a high % of yield and then further cycles gave lower percentage of yield for coupling products (Fig. 8b).

Cytotoxicity of CPTBH-PdNPs on MDA-MB-231 cell line

The MDA-MB-231 epithelial cancer cell line, was originated from an effusion of the pleura of a Caucasian lady (51-years-old) with metastatic mammary adenocarcinoma, is one of the commonly used breast cancer cell lines in therapeutic research (Cailleau et al. 1978). In the current research, calix[4]pyrrole tetrabenzohydrazide functionalized palladium nanoparticles were investigated for above mentioned cell line by means of in vitro studies using MTT assay. The assessment criterion was a half-maximal inhibitory concentration (IC_{50}) value and promising results (Table 5) were achieved for the CPTBH-PdNPs. Herein, the death of cancerous cells is the factor of success of the study, for that cell death is indicated by changes in the morphology of the cells (Yu-Guo Yuan and Gurunathan 2017). Figure 9 illustrates the acute changes in cell morphology that occurred when CPTBH-PdNPs concentration increased in contrast to the control (Fig. 9a). A larger empty space that is seen in the plates at higher CPTBH-PdNPs concentrations (Fig. 9f, g) displays a reduction in cells size, shape to spherical, clustering of cells, detachment of cells from the plate and eventually more cell deaths. Fani et al. displayed the antiproliferative study of cisplatin drug against MDA-MB-231 cell line and found a value of IC_{50} 1.3 ± 0.61 µg/mL (Fani 2016).

The possible mechanism of action of palladium nanoparticles in cancerous cells death is enigmatic (Al-Enazi et al. 2023) but, it may follow one or more paths of cell death, probably; generation of ROS (Reactive Oxygen Species) or causing nuclear fragmentation, or DNA rupture, membrane blebbing correlated with apoptosis, etc.(Carvalho Lopes and Pereira Torres 2020; Phan et al. 2020). Apart from this, few studies reveal the employability of palladium nanoparticles in cancer treatments. Recently, Liu et al. designed a Graphdiyne-templated PdNPs-based oxygen generator that reduced tumor hypoxia and slowed the development of tumors while maintaining high activity and stability, MDA-MB-231, A549, a squamous cell lung cancer xenograft model, and a 4T1 breast cancer xenografted mice model were the cell lines adopted for the investigation (Liu et al. 2020). Meanwhile, Kongor et al. produced nano-gold and

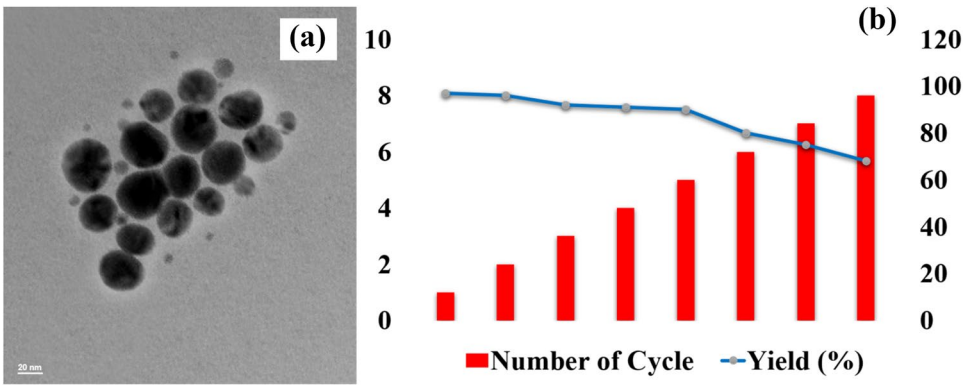

Fig. 8 **a** TEM image of aggregation of CPTBH-PdNPs after 5th cycle of catalysis and **b** recyclability chart of CPTBH-PdNPs

Table 5 Various concentrations and IC_{50} value of CPTBH-PdNPs against MDA-MB-231 cell line

CELL VIABILITY OF MDA-MB-231						
Concentration (µg/mL)	CPTBH-PdNPs			Doxorubicin		
100	*14.55*	*13.91*	*14.00*	14.93	14.70	14.85
50	*26.62*	*27.08*	*26.90*	37.56	37.71	37.40
25	58.74	59.19	58.92	43.23	43.00	43.16
12.5	64.50	64.14	64.32	46.42	46.50	46.58
6.2	76.03	76.40	76.12	46.81	46.89	46.73
3.125	85.18	85.73	85.64	47.90	47.67	47.82
Negative control	100			100		
IC_{50} value (µg/mL)	*38.86*			1.29		
Standard deviation	≤ 0.05			0.04		

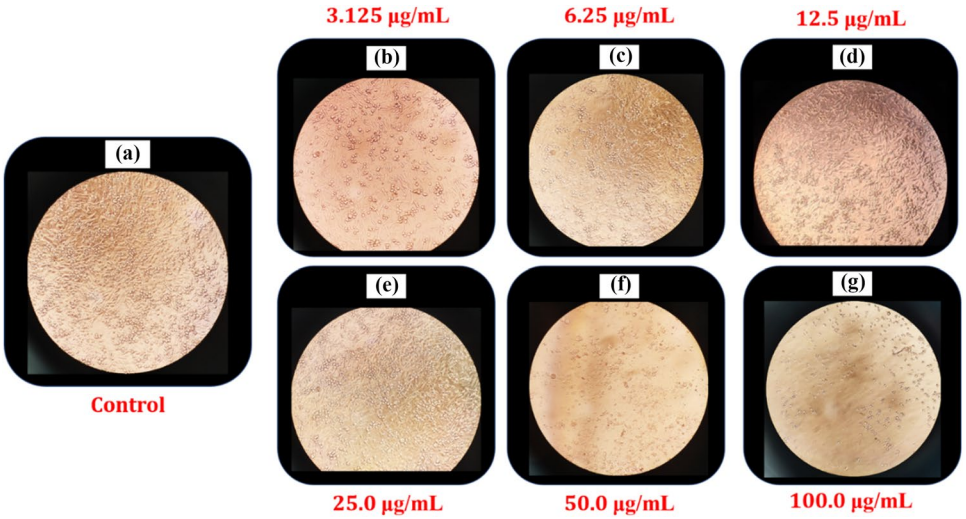

Fig. 9 **a** Control and **b**–**g** cytotoxicity of CPTBH-PdNPs on MDA-MB-231 cells

nano-silver capping by calixpyrrole have given results for the MCF-7 and HeLa cells, drawing IC_{50} values of 25.69 and 80 µg/mL, respectively (Kongor 2018a, 2020). Additionally, Table 6 shows a comparative list of palladium nanoparticles (with IC_{50} values or % cell viability) that are utilized as cytotoxic agents on different carcinoma cell lines.

Anti-tuberculosis effect of CPTBH-PdNPs

In current treatment of tuberculosis, antibiotics such as isoniazid, ethambutol, pyrazinamide, rifampicin are used as first-line therapy for the period of 6–9 months, after that in case of relapse second line of therapy is generally employed for the 18–24 months. Even though, above agents are very well known and has given excellent results to treat TB, there are cases where MDR-TB and XDR-TB observed (Tăbăran et al. 2020). However, to combat TB, the use of MNPs, significantly in this report, CPTBH-PdNPs has given exquisite results for the concentration range from 100 to 0.8 µg/mL (Fig. 10) using Microplate Alamar Blue assay (MABA), and turned out to be sensitive for whole range of concentration. To compare the outcomes of CPTBH-PdNPs, a first-line standard drugs were tested against *Mycobacteria tuberculosis* which offered findings as shown in Table 7.

Traditional anti-TB medications are more selective in TB treatment, but they require higher doses, which can have harmful side effects on patients and lead to drug resistance (Seung et al. 2015). Moreover, these medications are limited to single path for mechanism of action upon microbes, while Metal nanoparticles can interact with microbes through a variety of different paths, including morphology disruption, restriction of DNA replications, deactivating enzymes, DNA segmentation, etc. (Richa Singh et al. 2016). Table 8 illustrates the comparison of MIC values of different MNPs upon *Mycobacterium tuberculosis.*

Conclusion

Due to the numerous applications of C–C coupling compounds, the search for promising results in the Suzuki–Miyaura cross-coupling reactions is still urgently

Table 6 Cytotoxicity of palladium nanoparticles on different cancer cell lines

S. no.	Metal nanoparticle	Cell line	IC_{50}/cell viability (%)	References
1	Biological synthesized PdNPs	MDA-MB-231	8 µM	(Yu-Guo Yuan and Gurunathan 2017)
2	Biological synthesized PdNPs	MCF-7	104.79 µg/mL	(Al-Fakeh et al. 2021)
3	Polymer functionalized PdNPs	MCF-7	120 µg/mL	(Ramalingam et al. 2020)
4	Green synthesized PdNPs	MDA-MB-231	31.175 µg/mL	(Gulbagca et al. 2021)
5	Microwave assisted synthesized PdNPs	MDA-MB-231, HepG2, HeLa cells	40%, 52%, 38% (On addition of 100 µg/mL for all cases)	(Shivakumar et al. 2021)
6	Neem gum coated PdNPs	A549	45.6 ± 0.25 µg/mL	(Prakashkumar et al. 2021)
7	Green PdNPs	MCF-7	36.26 ± 0.91%	(Rokade et al. 2018)
8	Calix[4]pyrroletetrabenzohydrazide-PdNPs	MDA-MB-231	38.86 µg/mL	Current study

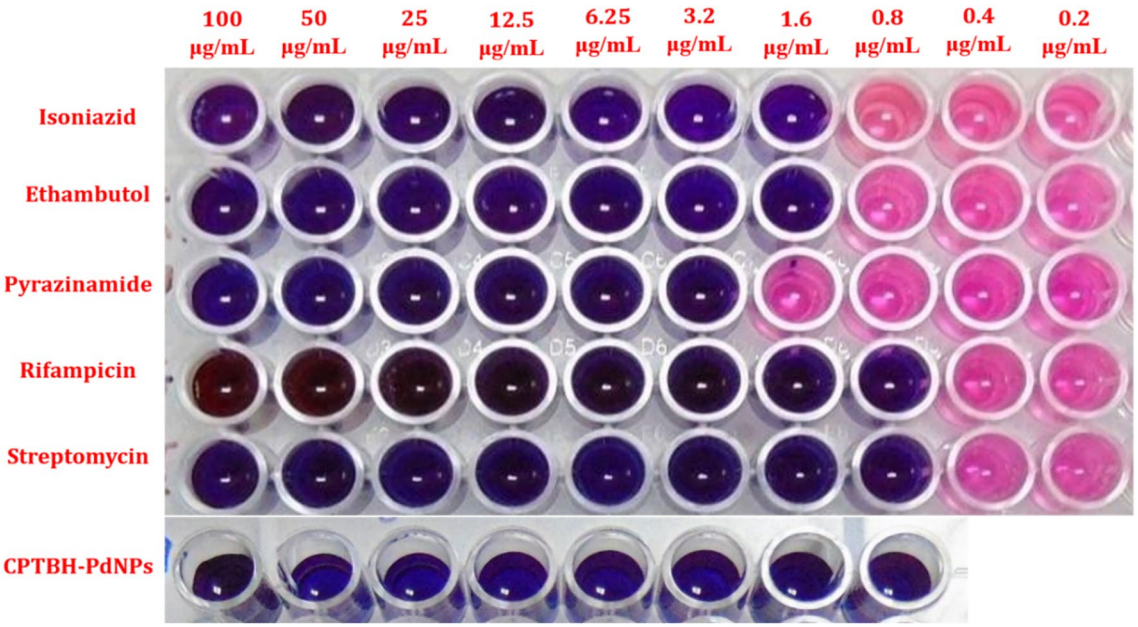

Fig. 10 Anti-tuberculosis effect of different standard drugs and CPTBH-PdNPs using distinct concentrations

Table 7 MIC values of various agents against Mycobacteria tuberculosis (H37RV strain)

S. no.	Anti-TB agent	Result in µg/mL
1	Isoniazid	1.6
2	Ethambutol	1.6
3	Pyrazinamide	3.125
4	Rifampicin	0.8
5	Streptomycin	0.8
6	CPTBH-PdNPs	0.8

needed in science. CPTBH-PdNPs have demonstrated competence in this regard with 0.008 mmol amount of catalyst at 80 °C, in DMF solvent, and yielded above 90% in all synthesized compounds. Additionally, CPTBH-PdNPs were used to assess for cytotoxicity on the MDA-MB-231 cell line by MTT test and have plausible outcomes with an IC_{50} value of 38.86 µg/mL, in conjunction efficacy of CPTBH-PdNPs on *Mycobacterium tuberculosis* was examined over wide concentration and found sensitive till 0.8 µg/mL which may be considered to be an efficient substitute as a future chemotherapeutic agent and antitubercular agent when combined with conventional medications and therapies after further study.

Supporting Information Summary

Supporting Information includes the characterization data of ESI–MS, FT-IR, and NMR of synthesized ligands (CPTBA and CPTBH) and Suzuki–Miyaura C–C coupling products.

Table 8 Comparison of MIC of different MNPs upon *Mycobacterium tuberculosis* with CPTBH-PdNPs

S. no.	Metal nano particles	MIC/cell viability (%)	References
1	ZnONPs	12.5 µg/mL	(Gopala Krishna et al. 2017)
2	Silver (AgNPs), gold (AuNPs), and gold–silver bimetallic (Au–AgNPs)	0.02–2.56 µg/mL	(Richa Singh et al. 2016)
3	Green Synthesized AuNPs	2.5 µg/mL & 20 µg/mL	(Arti Gupta et al. 2019)
4	Alginate-Capped AgNPs	4.17 ± 1.04 µg/mL	(Chen 2021)
5	Biosynthesized AuNPs	MIC_{99} at 6.42 µg/mL	(Priya et al. 2022)
6	Biosynthesized ZnNPs	1.25 µg/mL	(Punjabi et al. 2018)
7	Calix[4]pyrroletetrabenzohydrazide-PdNPs	0.8 µg/mL	Current Study

Supplementary Information The online version contains supplementary material available at https://doi.org/10.1007/s13204-023-02970-8.

Acknowledgements We are eternally grateful to the Department of Chemistry, Atmiya University, Rajkot, Gujarat for assisting in performing the synthesis of various organic compounds. We are extremely thankful to the Department of Chemistry, Tolani College of Arts and Science, Adipur-Kutch, and Ganpat University-CARS for providing facility for the analysis of samples.

Declarations

Conflict of interest There is no competing interest declared by authors.

References

Aksoy YT, Liu L, Abboud M, Vetrano MR, Koos E (2023) Role of nanoparticles in nanofluid droplet impact on solid Surfaces. Langmuir 39:12–19. https://doi.org/10.1021/acs.langmuir.2c02578

Al-Enazi NM, Alsamhary K, Kha M, Ameen F (2023) In vitro anticancer and antibacterial performance of biosynthesized Ag and Ce co-doped ZnO NPs. Bioprocess Biosyst Eng 46:89–103. https://doi.org/10.1007/s00449-022-02815-8

Al-Fakeh MS, Osman SO, Gassoumi M, Rabhi M, Omer M (2021) Characterization, antimicrobial and anticancer properties of palladium nanoparticles biosynthesized optimally using saudi propolis. Nanomaterials. https://doi.org/10.3390/nano11102666

Alzahabi KH, Usmani O, Georgiou TK, Ryan MP, Robertson BD, Tetley TD, Porter AE (2020) Approaches to treating tuberculosis by encapsulating metal ions and anti-mycobacterial drugs utilizing nano- and microparticle technologies. Emerging Topics in Life Sciences 4:581–600. https://doi.org/10.1042/ETLS20190154

Arti Gupta SP, Variya B, Shah S, Yadav JS (2019) Green synthesis of gold nanoparticles using different leaf extracts of ocimum gratissimum linn for anti-tubercular activity. Current Nanomed 9:146–157. https://doi.org/10.2174/2468187308666180807125058

Ayogu JI, Onoabedje EA (2021) Prospects and applications of palladium nanoparticles in the cross-coupling of (hetero)aryl halides and related analogues. ChemistryOpen 10:430–450. https://doi.org/10.1002/open.202000309

Bandyopadhyay A, et al (2020) Cytotoxic effect of green synthesized silver nanoparticles in MCF7 and MDA-MB-231 human breast cancer cells in vitro. Nucleus 63:191–202. https://doi.org/10.1007/s13237-019-00305-z

Banerjee PP et al (2019) Cytotoxic effect of graphene oxide-functionalized gold nanoparticles in human breast cancer cell lines. Nucleus 62:243–250. https://doi.org/10.1007/s13237-019-00284-1

Barhoum A, García-Betancourt ML, Rahier H, Van Assche G (2018) Physicochemical characterization of nanomaterials: polymorph, composition, wettability, and thermal stability. In: Barhoum A, Makhlouf ASH (eds) Emerging applications of nanoparticles and architecture nanostructures. Elsevier, pp 255–278. https://doi.org/10.1016/B978-0-323-51254-1.00009-9

Bedford RB, Cazin CSJ (2001) Highly active catalysts for the Suzuki coupling of aryl chlorides. Chem Commun. https://doi.org/10.1039/B105394A

Bhatt KD, Vyas DJ, Makwana BA, Darjee SM, Jain VK (2014) Highly stable water dispersible calix[4]pyrrole octa-hydrazide protected gold nanoparticles as colorimetric and fluorometric chemosensors for selective signaling of Co(II) ions. Spectrochim Acta Part A Mol Biomol Spectrosc 121:94–100. https://doi.org/10.1016/j.saa.2013.10.076

Bhatt KD, Vyas DJ, Makwana BA, Darjee SM, Jain VK, Shah H (2016) Turn-on fluorescence probe for selective detection of Hg(II) by calixpyrrole hydrazide reduced silver nanoparticle: application to real water sample. Chin Chem Lett 27:731–737. https://doi.org/10.1016/j.cclet.2016.01.012

Bhatt KD, Modi K, Kongor A (2021) Coupling reactions by highly efficient octacalix[4]pyrrole wrapped scrupulous nano-palladium catalyst. Biointerface Res Appl Chem 11:7632–7645. https://doi.org/10.33263/BRIAC111.76327645

Budarin V, Shuttleworth P, Clark J, Luque R (2010) Industrial applications of C–C coupling reactions. Curr Org Synth 7:614–627. https://doi.org/10.2174/157017910794328529

Cailleau R, Olivé M, Cruciger QVJ (1978) Long-term human breast carcinoma cell lines of metastatic origin: preliminary characterization. In Vitro 14:911–915. https://doi.org/10.1007/BF02616120

Carvalho Lopes J, Pereira Torres ML (2020) Utilização de Nanopartículas no Tratamento do Câncer: Aspectos Gerais, Mecanismos de Ação Antineoplásicos e Aplicabilidades Tumorais Revista Brasileira de Cancerologia 65:e-13400. https://doi.org/10.32635/2176-9745.RBC.2019v65n4.400.

Chatterjee S, Bhattacharya SK (2018) Size-dependent catalytic activity and fate of palladium nanoparticles in Suzuki-Miyaura coupling reactions ACS. Omega 3:12905–12913. https://doi.org/10.1021/acsomega.8b01598

Chen A, Ostrom C (2015) Palladium-based nanomaterials: synthesis and electrochemical applications. Chem Rev 115:11999–12044. https://doi.org/10.1021/acs.chemrev.5b00324

Chen L, Lang H, Fang L, Yu J, Wang L (2014) Nickel-catalyzed desulfitative Suzuki–Miyaura cross-coupling of N,N-disulfonylmethylamines and arylboronic acids. Eur J Org Chem 2014:6385–6389. https://doi.org/10.1002/ejoc.201402919

Chen CC, Chen YY, Yeh CC, Hsu CW, Yu SJ, Hsu CH, Wei TC, Ho SN, Tsai PC, Song YD, Yen HJ (2021) Alginate-capped silver nanoparticles as a potent anti-mycobacterial agent against mycobacterium tuberculosis. Front Pharmacol 12:746496. https://doi.org/10.3389/fphar.2021.746496

Chen X, Zang W, Vimalanathan K, Iyer KS, Raston CL (2013) A versatile approach for decorating 2D nanomaterials with Pd or Pt nanoparticles. Chem Commun 49:1160–1162. https://doi.org/10.1039/C2CC37606G

Creighton JA, Eadon DG (1991) Ultraviolet–visible absorption spectra of the colloidal metallic elements. J Chem Faraday Trans 87:3881–3891. https://doi.org/10.1039/FT9918703881

Cristoforetti G, Pitzalis E, Spiniello R, Ishak R, Muniz-Miranda M (2011) Production of Palladium nanoparticles by pulsed laser ablation in water and their characterization. J Phys Chem C 115:5073–5083. https://doi.org/10.1021/jp109281q

Desai AL, et al (2022) Calix[4]pyrrole based scrupulous probe for track on of tryptophan: Host-guest interaction, in silico modeling and molecular docking insights. Chem Phys 554:111426. https://doi.org/10.1016/j.chemphys.2021.111426

Fani S, et al. (2016) Anticancer activity of a monobenzyltin complex C1 against MDA-MB-231 cells through induction of Apoptosis and inhibition of breast cancer stem cells. Sci Rep 6:38992. https://doi.org/10.1038/srep38992

Gil Y-G, Kang S, Chae A, Kim Y-K, Min D-H, Jang H (2018) Synthesis of porous Pd nanoparticles by therapeutic chaga extract for highly efficient tri-modal cancer treatment. Nanoscale 10:19810–19817. https://doi.org/10.1039/C8NR07172A

Gopala Krishna P et al (2017) Antitubercular activity of ZnO nanoparticles prepared by solution combustion synthesis using lemon juice as bio-fuel. Mater Sci Eng, C 75:1026–1033. https://doi.org/10.1016/j.msec.2017.02.093

Gulbagca F, Aygün A, Gülcan M, Ozdemir S, Gonca S, Şen F (2021) Green synthesis of palladium nanoparticles: Preparation,

characterization, and investigation of antioxidant, antimicrobial, anticancer, and DNA cleavage activities. Appl Organometal Chem 35:e6272. https://doi.org/10.1002/aoc.6272

Guleria A, et al (2023) Solvated electron-induced synthesis of cyclodextrin-coated Pd nanoparticles: mechanistic, catalytic, and anticancer studies Dalton Trans 52:1036–1051. https://doi.org/10.1039/D2DT03219H

Ha J-M, Katz A, Drapailo AB, Kalchenko VI (2009) Mercaptocalixarene-capped gold nanoparticles via postsynthetic modification and direct synthesis: effect of calixarene cavity-metal interactions. J Phys Chem C 113:1137–1142. https://doi.org/10.1021/jp808165f

HironaoSajiki TK, Kozaki A, Zhang G, Kitamura Y, Maegawa T, Hirota K (2005) Efficient protocol for the phosphine-free Suzuki–Miyaura reaction catalyzed by palladium on carbon at room temperature. Synthesis 4:537–542. https://doi.org/10.1055/s-2004-837298

Hong K et al (2020) Palladium nanoparticles on assorted nanostructured supports: applications for Suzuki Heck, and Sonogashira cross-coupling reactions. ACS Appl Nano Mater 3:2070–2103. https://doi.org/10.1021/acsanm.9b02017

Hwang C-B, Fu Y-S, Lu Y-L, Jang S-W, Chou P-T, Wang CRC, Yu SJ (2000) Synthesis, characterization, and highly efficient catalytic reactivity of suspended palladium nanoparticles. J Catal 195:336–341. https://doi.org/10.1006/jcat.2000.2992

Jamkhande PG, Ghule NW, Bamer AH, Kalaskar MG (2019) Metal nanoparticles synthesis: an overview on methods of preparation, advantages and disadvantages, and applications. J Drug Deliv Sci Technol 53:101174. https://doi.org/10.1016/j.jddst.2019.101174

Javed R, Ain N, Gul A, Arslan Ahmad M, Guo W, Ao Q, Tian S (2022) Diverse biotechnological applications of multifunctional titanium dioxide nanoparticles: an up-to-date review. IET Nanobiotechnol 16:171–189. https://doi.org/10.1049/nbt2.12085

Kongor AR, Mehta VA, Modi KM, Panchal MK, Dey SA, Panchal US, Jain VK (2016) Calix-based nanoparticles: a review. Top Curr Chem 374:28. https://doi.org/10.1007/s41061-016-0029-z

Kongor A, et al (2018a) Selective fluorescence sensing of Cu(II) ions using calix[4]pyrrole fabricated Ag nanoparticles: a spectroscopic and computational approach. J Mol Liq 269:467–475. https://doi.org/10.1016/j.molliq.2018.08.014

Kongor A, et al (2020) Colorimetric and electrochemical sensing of As(III) using calix[4]pyrrole capped gold nanoparticles and evaluation of its cytotoxic activity. J Inclusion Phenomena Macrocycl Chem 98:29–41. https://doi.org/10.1007/s10847-020-01005-x.

Kongor A, Panchal M, Athar M, Mehta V, Bhatt K, Jha PC, Jain V (2018b) Heterogeneous hydrogenation using stable and reusable calix[4]pyrrole fenced Pt nanoparticles and its mechanistic insight. Appl Surf Sci 437:195–201. https://doi.org/10.1016/j.apsusc.2017.12.172

Kongor A, Panchal M, Athar M, Bhatt K, Jha PC, Jain V (2019) Facile construction of calix[4]pyrrole-templated gold nanoparticles: computational insights and application for efficient reduction of 4-nitrophenol. Gold Bull 52:125–133. https://doi.org/10.1007/s13404-019-00265-x

Kotha S, Lahiri K, Kashinath D (2002) Recent applications of the Suzuki–Miyaura cross-coupling reaction in organic synthesis. Tetrahedron 58:9633–9695. https://doi.org/10.1016/S0040-4020(02)01188-2

Liu J et al (2018) Palladium nanoparticles anchored on amine-functionalized silica nanotubes as a highly effective catalyst. J Phys Chem C 122:2696–2703. https://doi.org/10.1021/acs.jpcc.7b10237

Liu J et al (2020) Graphdiyne-templated palladium-nanoparticle assembly as a robust oxygen generator to attenuate tumor hypoxia. Nano Today 34:100907. https://doi.org/10.1016/j.nantod.2020.100907

Liu J et al (2021) Palladium nanoparticles on covalent organic framework supports as catalysts for Suzuki-Miyaura cross-coupling reactions. ACS Appl Nano Mater 4:6239–6249. https://doi.org/10.1021/acsanm.1c01038

Lourenco MC, de Souza MV, Pinheiro AC, Ferreira MdL, Gonçalves RS, Nogueira TCM, Peralta MAJA (2007) Evaluation of anti-tubercular activity of nicotinic and isoniazid analogues. ARKIVOC 15:181–191

Marziale AN, Faul SH, Reiner T, Schneider S, Eppinger J (2010) ChemInform abstract: facile palladium catalyzed Suzuki–Miyaura coupling in air and water at ambient temperature. ChemInform. https://doi.org/10.1002/chin.201021085

Mehta V, Panchal M, Kongor A, Panchal U, Jain VK (2016) Synthesis of water-dispersible Pd nanoparticles using a novel oxacalixarene derivative and their catalytic application in C–C coupling reactions. Catal Lett 146:1581–1590. https://doi.org/10.1007/s10562-016-1781-y

Melina Arnold EM, Rumgay H, Mafra A, Singh D, Laversanne M, Vignat J, Gralow JR, Cardoso F, Siesling S, Soerjomataram I (2022) Current and future burden of breast cancer: global statistics for 2020 and 2040. Breast 66:15–23. https://doi.org/10.1016/j.breast.2022.08.010

Merk H, Ködmön C, van der Werf MJ (2019) Will we reach the Sustainable Development Goals target for tuberculosis in the European Union/European Economic Area by 2030? Eurosurveillance 24:1–4. https://doi.org/10.2807/1560-7917.ES.2019.24.12.1900153

Miyaura N (2002) Organoboron Compounds. In: Miyaura N (ed) Cross-coupling reactions: a practical guide. Springer, Berlin Heidelberg, pp 11–59. https://doi.org/10.1007/3-540-45313-X_2.

Modi K, Patel C, Panchal U, Liska A, Kongor A, Jiri L, Jain VK (2019) Facile construction & modeling of a highly active thiacalixphenyl[4]arene-protected nano-palladium catalyst for various C-C cross-coupling reactions. New J Chem 43:5611–5622. https://doi.org/10.1039/C8NJ05866K

Mukhopadhyay S, Ratner S, Spernat A, Qafisheh N, Sasson Y (2002) Heterogeneous Pd-catalyzed biphenyl synthesis under moderate conditions in a solid−liquid two-phase system. Org Process Res Dev 6:297–300. https://doi.org/10.1021/op010047k

Narkhede N, Uttam B, Rao CP (2019) Calixarene-assisted Pd nanoparticles in organic transformations: synthesis, characterization, and catalytic applications in water for C–C coupling and for the reduction of nitroaromatics and organic dyes ACS. Omega 4:4908–4917. https://doi.org/10.1021/acsomega.9b00095

Nemamcha A, Rehspringer J-L, Khatmi D (2006) Synthesis of palladium nanoparticles by sonochemical reduction of palladium(II) nitrate in aqueous solution. J Phys Chem B 110:383–387. https://doi.org/10.1021/jp0535801

Newman JDS, Blanchard GJ (2006) Formation of gold nanoparticles using amine reducing agents. Langmuir 22:5882–5887. https://doi.org/10.1021/la060045z

Othman H, et al (2020) Antileukemic effect of palladium nanoparticles mediated by white tea *Camellia sinensis* extract in vitro and in WEHI-3B-induced leukemia in vivo. Evid-Based Complem Altern Med 2020:8764096. https://doi.org/10.1155/2020/8764096

Panchal U, Modi K, Panchal M, Mehta V, Jain VK (2016) Catalytic activity of recyclable resorcinarene-protected antibacterial Pd nanoparticles in C–C coupling reactions. Chin J Catal 37:250–257. https://doi.org/10.1016/S1872-2067(15)61021-X

Panchal M, Kongor A, Mehta V, Vora M, Bhatt K, Jain V (2018) Heck-type olefination and Suzuki coupling reactions using highly efficient oxacalix[4]arene wrapped nanopalladium catalyst. J Saudi Chem Soc 22:558–568. https://doi.org/10.1016/j.jscs.2017.09.006

Percec V, Bae J-Y, Hill DH (1995) Aryl mesylates in metal catalyzed homocoupling and cross-coupling reactions. 2 Suzuki-type nickel-catalyzed cross-coupling of aryl arenesulfonates and aryl

mesylates with arylboronic acids. J Organ Chem 60:1060–1065. https://doi.org/10.1021/jo00109a044

Pérez Y, Ruiz-González ML, González-Calbet JM, Concepción P, Boronat M, Corma A (2012) Shape-dependent catalytic activity of palladium nanoparticles embedded in SiO2 and TiO2. Catal Today 180:59–67. https://doi.org/10.1016/j.cattod.2011.09.011

Pérez-Lorenzo M (2012) Palladium nanoparticles as efficient catalysts for Suzuki cross-coupling reactions. J Phys Chem Lett 3:167–174. https://doi.org/10.1021/jz2013984

Phan TT, Huynh T-C, Manivasagan P, Mondal S, Oh J (2020) An up-to-date review on biomedical applications of palladium nanoparticles. Nanomaterials. https://doi.org/10.3390/nano10010066

Pomal NC, Bhatt KD, Modi KM, Desai AL, Patel NP, Kongor A, Kolivoška V (2021) Functionalized silver nanoparticles as colorimetric and fluorimetric sensor for environmentally toxic mercury ions: an overview. J Fluoresc 31:635–649. https://doi.org/10.1007/s10895-021-02699-z

Prakashkumar N, Vignesh M, Brindhadevi K, Phuong NT, Pugazhendhi A, Suganthy N (2021) Enhanced antimicrobial, antibiofilm and anticancer activities of biocompatible neem gum coated palladium nanoparticles. Progr Org Coat 151:106098

Priya MRK, Balasubramanian M, Nirmal CR, Dusthakeer A, Iyer PR (2022) Determination of anti-tuberculosis activity of biosynthesized gold nanocompounds against *M. tuberculosis* H37RV. Indian J Tuberculosis. https://doi.org/10.1016/j.ijtb.2022.09.002

Punjabi K, Mehta S, Chavan R, Chitalia V, Deogharkar D, Deshpande S (2018) Efficiency of biosynthesized silver and zinc nanoparticles against multi-drug resistant pathogens. Front Microbiol.

Ramalingam V, Raja S, Harshavardhan M (2020) In situ one-step synthesis of polymer-functionalized palladium nanoparticles: an efficient anticancer agent against breast cancer. Dalton Trans 49:3510–3518. https://doi.org/10.1039/C9DT04576G

Richa Singh LN, Arkile M, Wadhwani S, Shedbalkar U, Chopade S, Sarkar D, Chopade BA (2016) Phytogenic silver, gold, and bimetallic nanoparticles as novel antitubercular agents. Int J Nanomed 11:1889–1897. https://doi.org/10.2147/IJN.S102488

Rokade SS et al (2018) *Gloriosa superba* mediated synthesis of platinum and palladium nanoparticles for induction of apoptosis in breast cancer. Bioinorg Chem Appl 2018:4924186. https://doi.org/10.1155/2018/4924186

Seung KJ, Keshavjee S, Rich ML (2015) Multidrug-resistant tuberculosis and extensively drug-resistant tuberculosis. Cold Spring Harb Perspect Med 5:1–21. https://doi.org/10.1101/cshperspect.a017863. https://perspectivesinmedicine.cshlp.org/content/5/9/a017863

Shakil Hussain SM, Kamal MS, Hossain MK (2019) Recent developments in nanostructured palladium and other metal catalysts for organic transformation. J Nanomater 2019:1562130. https://doi.org/10.1155/2019/1562130

Shivakumar M, Manjunatha S, Dharmaprakash MS (2021) Biological activity of PdNPs derived from hemicellulose via microwave assisted green synthesis. Curr Res Green Sustain Chem 4:100150. https://doi.org/10.1016/j.crgsc.2021.100150

Tăbăran A-F, Matea CT, Mocan T, Tăbăran A, Mihaiu M, Iancu C, Mocan L (2020) Silver nanoparticles for the therapy of tuberculosis. Int J Nanomed 15:2231–2258. https://doi.org/10.2147/IJN.S241183

Thangavelu L et al (2022) Role of nanoparticles in environmental remediation: an insight into heavy metal pollution from dentistry. Bioinorg Chem Appl 2022:1946724. https://doi.org/10.1155/2022/1946724

Wang Y-C, Lai Y-R, Wu JW, Wang SSS, Lin K-S (2021) Using palladium nanoparticle-decorated lysozyme amyloid fibrils to catalyze the reduction of methylene blue. J Taiwan Inst Chem Eng 118:187–195. https://doi.org/10.1016/j.jtice.2020.12.030

(WHO) WHO (2023) Tuberculosis. WHO. https://www.who.int/news-room/fact-sheets/detail/tuberculosis#:~:text=Tuberculosis%20(TB)%20is%20an%20infectious,been%20infected%20with%20TB%20bacteria. Accessed 07/06/2023 2023

Yu-Guo Yuan Q-LP, Gurunathan S (2017) Combination of palladium nanoparticles and tubastatin—a potentiates apoptosis in human breast cancer cells: a novel therapeutic approach for cancer. Int J Nanomed 12:6503–6520. https://doi.org/10.2147/IJN.S136142